Adaptive Control System for Autonomous Helicopter Slung Load Operations

Bisgaard, Morten; la Cour-Harbo, Anders; Bendtsen, Jan Dimon

Published in:
Control Engineering Practice

DOI (link to publication from Publisher):
10.1016/j.conengprac.2010.01.017

Publication date:
2010

Document Version
Accepted author manuscript, peer reviewed version

Adaptive Control System for Autonomous Helicopter Slung Load Operations

Morten Bisgaard, Anders la Cour-Harbo, Jan Dimon Bendtsen

Department of Electronic Systems, Aalborg University, 9220 Aalborg East, Denmark, Fax: +45 98151739

Abstract

This paper presents design and verification of an estimation and control system for a helicopter slung load system. The estimator provides position and velocity estimates of the slung load and is designed to augment existing navigation in autonomous helicopters. Sensor input is provided by a vision system on the helicopter that measures the position of the slung load. The controller is a combined feedforward and feedback scheme for simultaneous avoidance of swing excitation and active swing damping. Simulations and laboratory flight tests show the effectiveness of the combined control system, yielding significant load swing reduction compared to the baseline controller.

Key words: Helicopter control, Delay, Feedforward control, Kalman filters, Autonomous vehicles, Frequency estimation

1. Introduction

A helicopter is a highly versatile aerial vehicle and its unique flying characteristics enable it to carry loads hanging in wires underneath the helicopter. Flying with an underslung load is known as either slung load or sling load flight and it is widely used for different kinds of cargo transport. However, flying a slung load can be a very challenging and sometimes hazardous task as a slung load significantly alters the flight characteristics of the helicopter. The pendulum-like behaviour of the slung load gives a high risk of pilot induced oscillations that can result in dangerous situations (Hoh et al. [12]). Furthermore, unstable oscillations can occur at high speeds due to the different aerodynamic shapes of the slung loads. There is therefore, from helicopter pilots and from the aerospace industry in general, a large interest in technologies that can address the challenge in operating helicopter slung loads.

The focus of this research is on enabling slung load flight in autonomous helicopters for general cargo transport. This is characterized by a suspension system that uses a single attachment point on the helicopter and by unknown slung load parameters. Furthermore, for general cargo transport there is no specific tracking requirement for the slung load, but stable flight must be ensured.

The contribution of this paper is the development of a control system that can be integrated on autonomous helicopters and thereby enable slung load flight for these. This is achieved through a three-step approach: First a slung load estimator capable of estimating the length of the suspension system together with the system states, and thereby allowing the model to be adapted, is designed using vision-based sensor data. The second step is the development of a feedforward control system based on input shaping that can be put on an existing autonomous helicopter and make it capable of performing manoeuvres with a slung load without inducing residual oscillations. The final and third step is to design a feedback control system to actively dampen oscillations of the slung load. Both the feedforward and feedback are designed to easily handle varying wire length and together with the adaptive slung load estimator they form an integrated control system as shown in figure 1. The

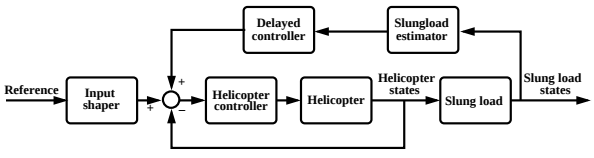

Figure 1: Architectural overview of the swing damping control scheme.

overall control concept is a classical cascaded scheme where the outer loop controller (the delayed feedback control) generates references to the inner loop controller (the helicopter controller). Where a traditional external reference input would be applied to the outer loop controller, it is here applied it to the inner loop. This means

that the reference input is a desired helicopter trajectory.

The control scheme presented here will only handles the lateral and longitudinal modes and while this is the primary influences Hoh et al. [12], the added slung load also affects the vertical helicopter dynamics. This was analysed for a helicopter / slung load mass ratio of 0.07 to 0.43 in Bisgaard [5] and the conclusion was that heave mode is almost unaffected by the slung load, but becomes a little slower as the mass ratio rises. It will be assumed that the helicopter controller is capable of handling the small change of heave mode bandwidth and includes an integration term that can handle the change in collective trim.

The paper starts with a review of previous work in control of helicopter slung load systems. Then the designs of the slung load state estimator, the feedforward and feedback controller are given. Finally, the full control scheme is verified through flight tests.

1.1. Previous Work

A number of different publications on control of helicopter slung load systems exist, but actual flight verification is very sparse in the literature. In Dukes [7] feedback from the load velocity to either main rotor thrust angles or to attachment point position is analyzed. It is concluded that feedback to rotor input gives only limited performance while feedback to the attachment point position is more advantageous. The problem of state estimation for slung load systems is mentioned in Dukes [8] and to overcome this problem an open loop control approach is suggested. This open loop control method resembles input shaping in the sense that the controller is designed such that excitation of the resonant modes is avoided, in this case by using appropriate spaced triangular pulses as control input. In Gupta and Bryson [11] an LQR controller is designed for a S-61 Sikorsky helicopter for near hover stabilization with a single wire suspension. SISO controllers are designed for the lateral and longitudinal axis taking wind disturbances into account. The problem of acquiring reliable measurements is discussed and it is suggested to use the angles of the suspension cable as sensor input to a linear Kalman filter. The resulting design is left untested, but stability and performance analysis shows satisfying results. An active control system mounted on the actual slung load is proposed in Raz et al. [20]. It consists of two vertical aerodynamic control surfaces intended to dampen oscillation on the load yaw and lateral axis in a single wire suspension system. Controller design is done using LQR and it is shown through linear analysis that the system is capable of stabilizing the system up to quite high airspeeds.

Robust control is used in Faille and Weiden [10] for stabilization of a helicopter with a point mass slung load. Controller design is done based on a reduced order linear model using $\mathcal{H}_\infty$ synthesis and it is shown through simulation to be able to stabilize the system. Receding Horizon Optimal control is suggested in Schierman et al. [23] and preliminary simulation results are presented. A recent publication is Oh et al. [18] which looks at a helicopter carrying a cable suspended robot that is controlled through a number of adjustable length cables. The nonlinear control design is done independently for the helicopter and for the load system and therefore relies on a controllable suspension system.

Twin lift system has also been the focus of some research through the past decades. In Rodriguez and Athans [22] a LQG control design is developed for a twin lift system with spreader bar and single load. The controller uses a master/slave configuration of the helicopters and simulations shows that the controller is capable of stabilizing the system and tracking velocity references. Robust control on a similar system is also applied in Reynolds and Rodriguez [21] where $\mathcal{H}_\infty$ is used and simulation is used to verify that the system can track velocity references. A feedback linearization scheme is presented in Mittal et al. [17] where a twin lift system without spreader bar is considered. The controller is designed to adapt to an unknown slung load mass and simulations is used to show that the system is stabilized by the controller.

For smaller scale helicopter the 1997 AUVSI International Aerial Robotics Competition showed autonomous flight with a slung load. The winning entry by Carnegie Mellon Miller et al. [16] demonstrated object collection by a controllable suspension system with PID controllers for helicopter and slung load system. Feedforward control was used to compensate for helicopter motion in the slung load control, while the helicopter controller was unaware of the slung load. Recently in Bernard et al. [4] autonomous helicopter slung load flight with both single and multiple small scale helicopters was demonstrated where force feedback from the load attachment was used.

2. Slung Load State Estimator

The purpose of the estimator is to provide estimates of the slung load states ($\hat{\boldsymbol{\chi}}_l, \dot{\hat{\boldsymbol{\chi}}}_l \in \mathbb{R}^3$). It is designed to augment an already existing inertial measurement unit (IMU) driven state estimator and it uses the estimated helicopter states ($\hat{\boldsymbol{\chi}}_h, \dot{\hat{\boldsymbol{\chi}}}_h \in \mathbb{R}^3 \times \mathbb{S}^3$) as well as the bias and gravity corrected acceleration measurements from the IMU ($\boldsymbol{a}_h$) as shown in figure 2. The estima-

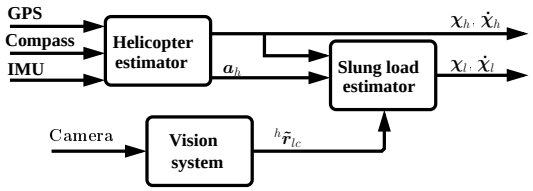

Figure 2: The architecture of the slung load state estimator.

tor uses a vision based system as the only sensor input and therefore it does not require any mounting of sensors on the load. The vision system uses images from a downwards looking camera to calculate a unit vector in the helicopter fixed frame pointing from the camera to the load. Furthermore the wire length is estimated online and therefore the estimator does not require exact knowledge of the suspension system. This makes it ideal for augmenting an already autonomous UAV with slung load capabilities.

2.1. Unscented Kalman Filter

An unscented Kalman filter (UKF) is used as the architecture for the state estimation. The UKF is a relative new approach to Kalman filtering which was first proposed in Julier and Uhlmann [13] and in recent years has been intensively researched for a wide range of estimation purposes. It has become quite popular, because it in theory yields higher precision than the extended Kalman filter (EKF), as it does not require first-order linear approximations. However, this advantage is in many cases more theoretical that practical as modelling uncertainties are often more significant than linearisation errors (Bisgaard et al. [6]). Nevertheless, the possibility of using the nonlinear process and sensor models directly in the filter is a large advantage in many cases. It should be noted that when using a computational expensive nonlinear model with many states, the UKF becomes computational expensive.

The UKF is based on the so-called unscented transformation, which is used to calculate mean and covariance values for a random variable through a deterministic sampling approach. This is done by propagating the system state vector, using a number of carefully selected sample points, through the nonlinear model to evaluate the mean and covariance of the state estimate. The number of selected sample points are equal to $2n + 1$ where n is the number of states and they are chosen to lie on a hypersphere around the state.

2.2. Process Model

The system is modeled as a 3-dimensional point mass pendulum as shown in figure 3 using a wire frame that is fixed at the wire attachment point and having the z-axis pointing along wire. This means that the position of the slung load in the wire frame is defined as

$$ {}^w\boldsymbol{l} = \begin{bmatrix} 0 & 0 & l \end{bmatrix}^T, \tag{1} $$

where l is the length of the wire. The position of the load in the wire fixed frame can is described by the generalized coordinates $({}^e\theta_w, {}^e\phi_w)$, which can be considered as a 2-1 Euler angle rotation around the attachment point. This means that the rotation from wire frame to earth frame can be written as

$$ \begin{aligned} \boldsymbol{T}_{we} &= \boldsymbol{T}_{ew}^T \\ &= \begin{bmatrix} 1 & 0 & 0 \\ 0 & \cos(\phi_w) & -\sin(\phi_w) \\ 0 & \sin(\phi_w) & \cos(\phi_w) \end{bmatrix} \begin{bmatrix} \cos(\theta_w) & 0 & -\sin(\theta_w) \\ 0 & 1 & 0 \\ \sin(\theta_w) & 0 & \cos(\theta_w) \end{bmatrix} \\ &= \begin{bmatrix} \cos(\theta_w) & 0 & -\sin(\theta_w) \\ -\sin(\phi_w)\sin(\theta_w) & \cos(\phi_w) & -\sin(\phi_w)\cos(\theta_w) \\ \cos(\phi_w)\sin(\theta_w) & \sin(\phi_w) & \cos(\phi_w)\cos(\theta_w) \end{bmatrix}, \end{aligned} \tag{2} $$

where it should be noted that the y-axis rotation $({}^e\theta_w)$ has a different sign definition compared to a standard Euler rotation.

The load position is described using earth fixed coordinates as this means that they are independent of the helicopter attitude changes. The double pendulum motion, created by the attitude of the load with respect to the wire, is neglected, i.e. the load is considered always to be aligned with the wire. Furthermore, the translational accelerations of the helicopter attachment point generated by angular motions are neglected.

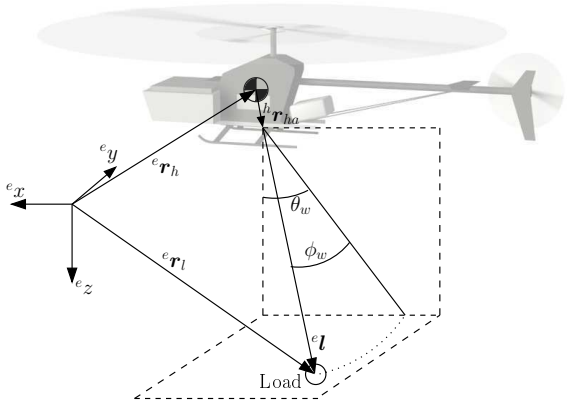

Figure 3: The point mass slung load model.

As mentioned earlier the slung load estimator is intended for augmenting an existing helicopter state estimator and is therefore assumed that an adequate filtering on the helicopter states have been performed. It is

therefore chosen to use the acceleration output of the helicopter estimator as input to the slung load model. Given the acceleration of the pendulum pivot point, the angular motion can be found as

$$\ddot{\boldsymbol{\theta}} = l^{-1\,w}\ddot{\boldsymbol{x}} = l^{-1}\boldsymbol{T}_{we}{}^{e}\ddot{\boldsymbol{x}} \tag{3}$$

where $\ddot{\boldsymbol{\theta}}$ is a vector of the angular accelerations and $\ddot{\boldsymbol{x}}$ is a vector of the translational acceleration (including gravity) and $l = |{}^{e}\boldsymbol{l}|$ is the length of the pendulum. Expanding yields

$$\begin{aligned} {}^{e}\ddot{\theta}_w =& (-\cos(\theta_w)\cos(\phi_w){}^{e}\ddot{x}_h + \\ & \sin(\theta_w)\cos(\phi_w)({}^{e}\ddot{z}_h - g))/l\,, \end{aligned} \tag{4}$$

$$\begin{aligned} {}^{e}\ddot{\phi}_w =& (\sin(\theta_w)\sin(\phi_w){}^{e}\ddot{x}_h - \cos(\phi_w){}^{e}\ddot{y}_h + \\ & \cos(\theta_w)\sin(\phi_w)({}^{e}\ddot{z}_h - g))/l\,, \end{aligned} \tag{5}$$

where $[\ddot{x}_h\ \ddot{y}_h\ \ddot{z}_h]^T$ are the helicopter translational accelerations. The position of the load in the earth fixed frame can be found from figure 3 as

$${}^{e}\boldsymbol{r}_l = {}^{e}\boldsymbol{l} + {}^{e}\boldsymbol{r}_h + \boldsymbol{T}_{eh}{}^{h}\boldsymbol{r}_{ha}\,, \tag{6}$$

and load velocities can be found as the differentiation of (6).

2.3. Sensor Model

The output of the vision system is a unit vector (${}^{h}\tilde{\boldsymbol{r}}_{lc}$) pointing towards the load from the camera as shown on figure 4. The estimated position of the load relative to

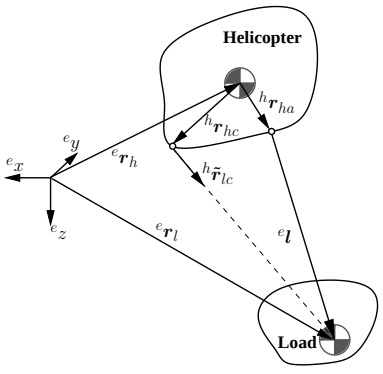

Figure 4: The geometric setup of the sensor model.

the helicopter attachment point (${}^{e}\hat{\boldsymbol{l}}$) can be found from (1) and (2) as

$${}^{e}\hat{\boldsymbol{l}} = \hat{\boldsymbol{T}}_{ew}{}^{w}\boldsymbol{l} = \begin{bmatrix} \sin(\hat{\theta}_w)\cos(\hat{\phi}_w) \\ \sin(\hat{\phi}_w) \\ \cos(\hat{\theta}_w)\cos(\hat{\phi}_w) \end{bmatrix} l\,, \tag{7}$$

The predicted measurement can then be found by offsetting this vector to the camera position (as shown on figure 4) and normalizing

$${}^{h}\hat{\boldsymbol{r}}_{lc} = \frac{\boldsymbol{T}_{he}{}^{e}\hat{\boldsymbol{l}} + {}^{h}\boldsymbol{r}_{ha} - {}^{h}\boldsymbol{r}_{hc}}{|\boldsymbol{T}_{he}{}^{e}\hat{\boldsymbol{l}} + {}^{h}\boldsymbol{r}_{ha} - {}^{h}\boldsymbol{r}_{hc}|}\,. \tag{8}$$

2.4. Vision System

The vision system is a camera mounted on the helicopter frame looking down on the load. The resulting image is a top-down view of the load and the ground below. To easily identify the load amongst other objects that appear in the camera view the load is fitted with a visual marker; in this case a white disk on a black background. The location of the marker in the image is thus an estimate of the position of the load relative to the orientation of helicopter.

To identify the marker in the image two circular Hough transforms with different radii are usedBallard [2]. A circular Hough transform maps a 2D data set into another 2D data set such that complete circles are mapped to single points. Since points can be found easily by, for instance, thresholding, it makes the search for circles much simpler. The first of the two transforms uses a radius slightly smaller than the white disc marker and triggers on white. The second transform uses a radius slightly bigger than the white disc marker and triggers on black. Correlating the two transforms triggers only those areas where a sufficiently large round white area is present and surrounded by a black area. This is sufficient to yield a good estimate of the marker location; as long as the image of the marker is good, i.e. not distorted by helicopter vibration, this method produces a sub-pixel precision estimate of the marker location. An image from a test flight is shown in figure 5.

Figure 5: Left: Input to the Hough transform; the slung load can be seen in the upper half of the picture. Right: Output of the Hough transform from which the load can be easily located by a peak detector.

The measurement is checked for a false detection by examining the pixel detected as the centre of the disk.

If it is not sufficiently white it is assumed that the algorithm has made a false detection and the measurement is discarded. This could happen if the load is outside the field of view (FOV) of the camera. Note that the camera is fixed to the helicopter which means that both load swing and helicopter roll and pitch can result in the load disappearing from FOV.

It is important to keep the delay in the vision system low and this is ensured by using the previous estimate of the location to choose a subset – a region of interest (ROI) – of the image for analysis in the next image frame. On top of that a threshold is used to simply ignore the pixels that are too far from white to be the maker. The size of the ROI is a trade-off where a smaller ROI yields a smaller FOV and therefore larger risk of the load disappearing from FOV, but at the same time a smaller ROI yields a faster update time on the vision algorithm which gives a smaller risk of the load disappearing from FOV.

When the vision algorithm has detected the pixel position of the load this measurement must be mapped to a 3D load position. This is done by first transforming the pixel position to two angles – a vertical (θ_p) and a horizontal (ϕ_p) – as shown in figure 6. The camera coordinate system is defined to coincide with the helicopter coordinate system when the camera is pointing forward, i.e. the x-axis is pointing in the image direction. This is

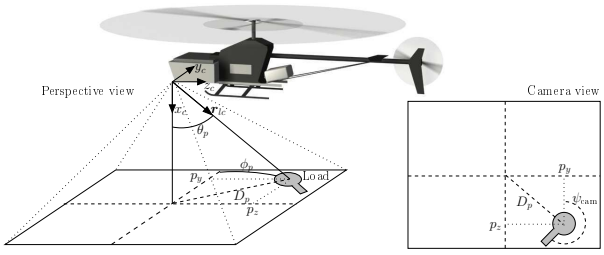

Figure 6: The map of 2D picture position to the 3D spatial location.

done by assuming that the angle from the camera to the load (θ_p) is proportional to the pixel distance from the load to the image center. This is equivalent to a pin-hole lens and neglects optical lens distortion. The distance from the image center to the load is found as

$$D_p = \sqrt{p_y^2 + p_z^2} \, . \tag{9}$$

The angle to the load can then be found as

$$\theta_p = \frac{\alpha_{\text{FOV}}}{P_{\text{FOV}}} D_p \, , \tag{10}$$

where α_{FOV} is the field of view angle of the camera and P_{FOV} is the number of pixels related to the α_{FOV}. The horizontal angle can be found simply by the relationship between the x and the y pixel position

$$\phi_p = \arctan(p_z / p_y) \, . \tag{11}$$

The unit vector from the camera to the load can then be found in the camera coordinate system and rotated into the helicopter coordinate system as

$${}^h\boldsymbol{r}_{cl} = \boldsymbol{T}_{hc} \begin{bmatrix} \cos(\theta_p) \\ \sin(\theta_p)\cos(\phi_p) \\ \sin(\theta_p)\sin(\phi_p) \end{bmatrix} \, , \tag{12}$$

where $\boldsymbol{T}_{hc}$ is the direct cosine matrix between the camera and the helicopter. The observability of the system is clear as the vision system directly measures the unit vector pointing to the slung load and the length of the vector can be calculated as show in the following.

2.5. Wire Length Estimation

The pendulous mode frequency of the dual mass helicopter slung load system can be determined as

$$\omega_n = \sqrt{\frac{g(m_h + m_l)}{l m_h}} \, . \tag{13}$$

However, if feedback control is applied to the helicopter, the dual mass system behaviour is altered as the effect of slung load swing on the helicopter is suppressed. The system can then be approximated by a standard pendulum description, which means that the wire length can then be calculated as

$$l = \frac{\omega_n^2}{g} \, . \tag{14}$$

This frequency is present as a slow sine wave in the measured load angles ($\tilde{\theta}_w$ and $\tilde{\phi}_w$), and could be estimated using standard FFT (note that it is important to use the measurements transformed into the earth fixed frame to remove helicopter motion from the signals). However, since it is known that the frequency is quite low and as it is desired to estimate the frequency quickly (i.e. using few samples), a dedicated sine estimator is used. This estimator is a steepest ascent search on (a discretized version of)

$$f(\omega, \theta) = \frac{\int_0^{2\pi} s(t)\cos(\omega t + \theta) dt}{\int_0^{2\pi} \cos^2(\omega t + \theta) dt} \, , \tag{15}$$

where $s(t)$ is the input signal. This function is the normalized inner product between the signal and a linearly independent (but non-orthogonal) cosine frame,

and thus peaks when ω matches the main frequency of the signal. This method is superior to the oversampled FFT when searching for one, approximately known frequency, partly because it involves significantly fewer computations and partly because the oversampled FFT does not include normalization at 'non-integer' frequencies.

However, it is important to use the wire length estimator with care: Around hover the oscillations may be so small that it is difficult to detect the correct frequency and when used in a closed loop system the frequency of the oscillation can be shifted depending on the controller. Therefore, the strategy for using the estimator is to make a gentle step with the helicopter shortly after take off which generates free swing of the slung load. When the sine estimator has converged after a short period of time, the wire length is locked to the found value and the state estimates are ready for use in close loop.

The step size of the steepest ascent is the best choice out of five different predetermined sizes. Typically, the method converges in 100 - 200 steps, which can be distributed over time as more signal becomes available to avoid high peak load on the computer.

3. Feedforward Control

Damping swing of a slung load is similar to vibration damping in many other applications and while actual examples of slung load anti swing control are rare in the literature, inspiration can be found in other applications. One of the most obvious applications to draw inspiration from is overhead gantry cranes, which exhibit the same pendulum like behaviour, albeit with much simpler actuator dynamics. A commonly used solution to the swing damping problem is input shaping. The concept of input shaping was first suggested in Smith [26]. The method was dubbed the Posicast technique and was based on the idea of exciting two transient oscillations in a underdamped system such that they cancel each other and thereby achieving an oscillation free response. Input shaping has been applied to a range of applications apart from cranes, including flexible robotic manipulators and space crafts with flexible solar arrays and fuel sloshing. A good introduction to input shaping techniques is given in Singh and Singhose [25], where a review of input shaping literature is given together with a tutorial to practical input shaping design.

A simple way of driving a system with vibration is by using impulses: An impulse A_1 is first applied to the system which will not only start a motion, but also cause a vibration. However, instead of allowing the system to vibrate, another impulse is applied at an appropriate time, which then cancels the vibration. The concept is illustrated in figure 7 with a undamped second order system with the natural frequency $\omega_n = 1$ rad/s.

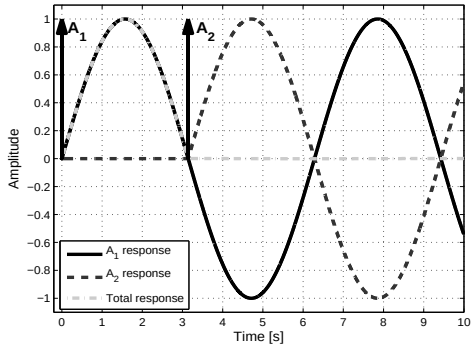

Figure 7: An undamped second order system driven by two impulses to achieve a zero vibration response.

To evaluate the performance of applying a sequence of impulses to cancel vibration a non-dimensional residual vibration term is defined as the vibration amplitude cause by impulse sequence normalized with the vibration amplitude cause by unit impulse evaluated at the time of last impulse in the sequence, which yields (Singh and Singhose [25])

$$\mathcal{V}(\omega_n, \zeta) = e^{\zeta\omega_n t_N} \sqrt{C(\omega_n, \zeta)^2 + S(\omega_n, \zeta)^2}\,, \qquad (16)$$

where

$$C(\omega_n, \zeta) = \sum_{i=1}^{N} A_i e^{\zeta\omega_n t_i} \cos(\omega_d t_i)\,, \qquad (17)$$

$$S(\omega_n, \zeta) = \sum_{i=1}^{N} A_i e^{\zeta\omega_n t_i} \sin(\omega_d t_i)\,, \qquad (18)$$

where ω_n is the natural frequency, ζ is the damping, and $\omega_d = \omega_n\sqrt{1-\zeta^2}$ is the damped frequency. To achieve a system response with zero residual vibration the impulse series $A_{1\ldots N}$ that satisfies $\mathcal{V} = 0$ in (16) must be found. The shortest possible shaper consists of two impulses which yields four unknowns: A_1, A_2, t_1, and t_2. Solving for these yields

$$t_1 = 0\,, \quad t_2 = \frac{T_d}{2}\,, \quad A_1 = \frac{1}{1+K}\,, \quad A_2 = \frac{K}{1+K}\,. \qquad (19)$$

where T_d is the period of the damped oscillation and

$$K = \exp\left(\frac{-\zeta\pi}{\sqrt{1-\zeta^2}}\right). \qquad (20)$$

3.1. Robust Zero Vibration Command Generation

In theory, the Zero Vibration (ZV) shaper is capable of successfully avoiding any oscillation when the natural frequency and damping of the system oscillatory modes are known. However, in reality, you never have exact system knowledge which means that there will often be a discrepancy between the actual system and the system used for the shaper design. Such a case is illustrated in figure 8 where the system from figure 7 how has a 5% error in the frequency. It is clear that while

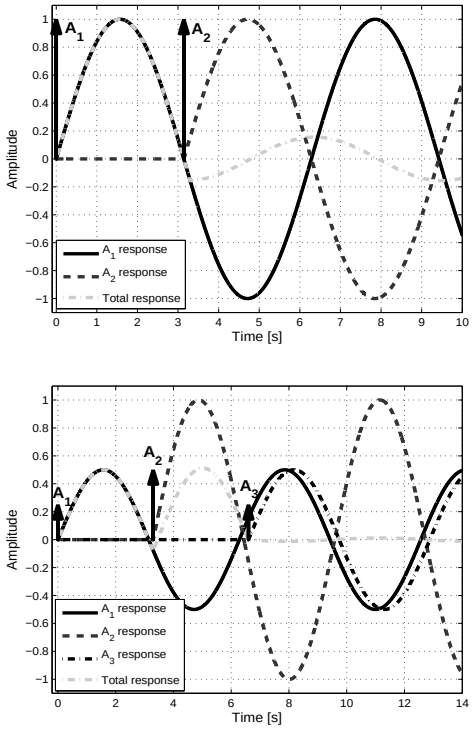

Figure 8: Response to ZV and robust ZV (ZVD) shaper with 5% frequency error.

the residual vibration is somewhat reduced there is still a significant amount of vibration left and the solution is to add robustness to the shaper (Singer [24]). This resulted in the ZVD shaper which is substantially more robust to modeling errors as shown to the right in figure 8. The shaper is derived by adding the requirement that the derivative (thus the D in ZVD) of the residual vibration with respect to the natural frequency and damping must be equal to zero

$$0 = \frac{d}{d\omega_n}\mathcal{V}(\omega_n,\zeta)\,, \qquad 0 = \frac{d}{d\zeta}\mathcal{V}(\omega_n,\zeta)\,. \tag{21}$$

This is achieved by adding an additional impulse to the two impulse ZV input shaper, which yields the three impulse ZVD input shaper. The solution to the ZVD shaper is Singer [24]

$$t_2 = \frac{T_d}{2}\,, \quad t_3 = T_d\,, \quad A_1 = \frac{1}{1+2K+K^2}\,,$$
$$A_2 = \frac{2K}{1+2K+K^2}\,, \quad A_3 = \frac{K^2}{1+2K+K^2}\,. \tag{22}$$

The zero derivative constraint makes the slope of the ZVD shaper zero at the natural frequency and thereby improving the robustness of the shaper to modeling errors. In figure 9 it is illustrated how robust the ZVD shaper are to errors in damping and frequency.

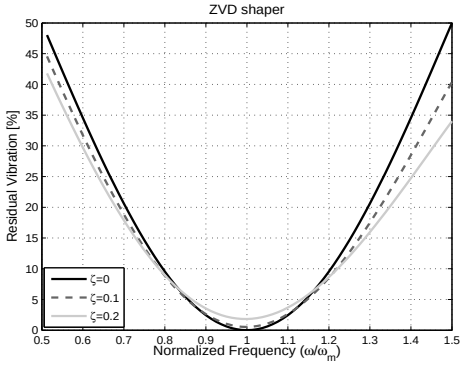

Figure 9: Robustness of the ZVD shaper as a function of error in damping (ζ) and frequency (ω_n).

3.2. Real-Time Input Shaping

Input shaping is implemented by convolving a sequence of impulses with any desired command as

$$\overset{*}{C}(t) = \mathcal{I} * C(t)\,, \tag{23}$$

where C is the initial command, $\mathcal{I}$ is the input shaper, and $\overset{*}{C}$ is the shaped command. By using a well designed input shaper, the system will respond to the shaped reference signal without vibration. An input shaper can therefore be used to filter the reference commands to the system such that, ideally, swing free motion of the slung load can be achieved.

However, there is a price to be paid for the reduced vibration that can be achieved by using the input shapers and especially the robust input shapers. When a command is convolved with an input shaper, the duration of the command is extended with the length of the shaper, as illustrated in figure 10. Therefore, it can generally by said that a longer shaper yields a slower system response. However, this prolonged response time is most significant for very short manoeuvre commands like a

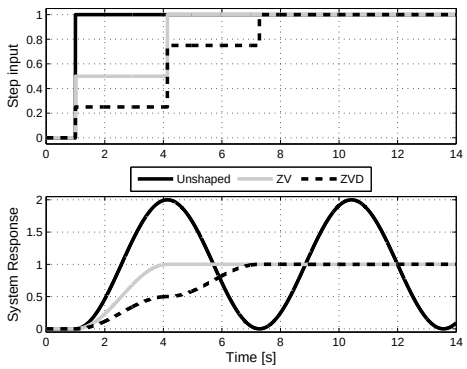

Figure 10: Step inputs and system response without shaping, with ZV and with ZVD shaping.

step. For longer manoeuvres like a flight trajectory for the helicopter slung load system, the additional response time added by the input shaper is insignificant.

3.3. Input Shaping for the Helicopter Slung Load

The use of the input shaper technique to reduce excitation of the slung load pendulous modes has the distinct advantage that there is no need to make preflight tuning of the controller. In section 2.5 it was demonstrated how it is possible to get estimates of the natural frequency of the pendulum mode. This estimate can be used directly in the input shaper, but is important to remember that the estimate represent the damped frequency of the system ω_d and provides no information on the damping ζ. The damping of the slung load motion will vary depending on the aerodynamic drag of the load and on the interaction with the helicopter. Given these uncertainties, a robust shaper seems like the better choice and from figure 9 it can be seen that the ZVD shaper seems quite robust to uncertainties especially in the damping and this shaper is therefore used for the system.

The input shaper is applied to the entire reference trajectory which is necessary for coordinated manoeuvres to keep the synchronization between the different elements. If the input shaper is only applied to parts of the reference vector, these will be delayed compared to the remaining elements.

4. Feedback Control

After having designed the feedforward controller that helps avoid exciting swing, a feedback controller for active damping of swing must now be found. A possibility for this is the so called delayed controller; the idea with the delayed controller is that by using intentionally delayed feedback it is possible to absorb vibrations in a oscillating system. Traditionally, delay in feedback systems is considered problematic and causes deteriorating performance and even instability, but in this approach the delay can be used as an advantage. It was first suggested in Olgac and Holm-Hansen [19] which consider vibration damping in structures where it was denoted 'Delayed Resonator'. The delayed resonator is designed as an oscillator with a natural frequency equal to that of the system, and with an appropriate delay this can be fed to the system and cancel the system vibrations. A comparison of the delayed resonator with a standard PD controller is made in Elmali et al. [9] and it is concluded that a comparable performance can be achieved with the two. However, the delayed feedback has a number of advantages over the PD controller, most prominently the ability to incorporate system delays into the controller without loss of performance. This is especially true in this case where slung load measurements are provided by a vision/image processing system which on systems with low computational power can result in long delays. In Masoud and Nayfeh [15] and Masoud et al. [14] the delayed resonator is used to dampen swing in ship cranes. Also Udwadia and Phohomsiri [27] extends the concept to consider both negative and positive feedback and applies it to vibration damping in structures.

4.1. Delayed Feedback Theory

A standard linear second order system is given by

$$\ddot{x}(t) + 2\omega_n\zeta\dot{x}(t) + \omega_n^2 x(t) = u(t)\,, \tag{24}$$

where ω_n is the natural frequency and ζ is the damping. A proportional feedback of the time delayed state value is introduced as

$$\ddot{x}(t) + 2\omega_n\zeta\dot{x}(t) + \omega_n^2 x(t) = G_d x(t-\tau_d)\,, \tag{25}$$

where design parameters of the controller are the gain G_d and the time-invariant delay τ_d. In the Laplace domain (25) becomes

$$x(s^2 + 2\omega_n\zeta s + \omega_n^2) = G_d e^{-\tau_d s}\,. \tag{26}$$

The controller parameters (G_d, τ_d) must now be found such that the damping of the system is maximised. More or less complicated approaches have been suggested in the literature for this see e.g. Masoud and Nayfeh [15]. However, a simple approach will be proposed here; model the delay using a Padé approximant (Baker Jr and Graves-Morris [1]). The Padé approximant is accurate in the magnitude but results in an error in the

phase. For a first order approximation the phase error is close to 5 degrees at the delay frequency while a second order approximation results in an error of around 2 degrees at twice the delay frequency. This is deemed an adequate accuracy for this control system and a second order Padé approximation is therefore used

$$e^{-\tau_d s} \simeq \frac{1 - \tau_d/2s + \tau_d^2/12s^2}{1 + \tau_d/2s + \tau_d^2/12s^2} , \tag{27}$$

and by using this approximation linear system theory can be applied to find the appropriate control parameters. The delayed feedback controller ($\boldsymbol{C}$) can be formulated in state space form as

$$\begin{aligned} \boldsymbol{C} &= \begin{cases} \dot{\boldsymbol{x}}_c &= \boldsymbol{A}_c\boldsymbol{x}_c + \boldsymbol{B}_c\boldsymbol{u}_c \\ \boldsymbol{y}_c &= \boldsymbol{C}_c\boldsymbol{x}_c + \boldsymbol{D}_c\boldsymbol{u}_c \end{cases} , \\ \boldsymbol{A}_C &= \begin{bmatrix} -6/\tau_d & -12/\tau_d^2 \\ 1 & 0 \end{bmatrix} , \boldsymbol{B}_C = \begin{bmatrix} G_d \\ 0 \end{bmatrix} , \\ \boldsymbol{C}_C &= \begin{bmatrix} -12G_d/\tau_d & 0 \end{bmatrix} , \boldsymbol{D}_C = 1 . \end{aligned} \tag{28}$$

4.2. Automated Design of the Delayed Feedback Controller

The purpose of the controller is to dampen the pendulous modes of the slung load within the limits of the helicopter performance. The design of the controller can then be formulated as finding the controller parameter set (G_d, τ_d) that achieves the maximum damping of the pendulous modes while maintaining satisfactory helicopter behaviour. The controllability of the system is evident from the fact that there is independent control of the helicopter along in x, y, and z.

Let the linear system

$$\boldsymbol{H} = \begin{cases} \dot{\boldsymbol{x}}_h &= \boldsymbol{A}_h\boldsymbol{x}_h + \boldsymbol{B}_h\boldsymbol{u}_h \\ \boldsymbol{y}_h &= \boldsymbol{C}_h\boldsymbol{x}_h + \boldsymbol{D}_h\boldsymbol{u}_h \end{cases} , \tag{29}$$

where $\boldsymbol{x} \in \mathbb{R}^n$ is the state vector, $\boldsymbol{u} \in \mathbb{R}^m$ is the input vector, and $\boldsymbol{y} \in \mathbb{R}^p$ is the output vector, be the combined helicopter slung load system. By applying the controller of (28) to the system in positive feedback, the combined dynamics can be found as

$$\boldsymbol{A}_t = \begin{bmatrix} \boldsymbol{A}_h & \boldsymbol{B}_h\boldsymbol{C}_c \\ \boldsymbol{B}_c\boldsymbol{C}_h & \boldsymbol{A}_c \end{bmatrix} , \quad \boldsymbol{x}_t = \begin{bmatrix} \boldsymbol{x}_h \\ \boldsymbol{x}_c \end{bmatrix} . \tag{30}$$

For this system the eigenvalues are given by

$$(\boldsymbol{A}_t - \boldsymbol{\lambda I})\boldsymbol{x}_t = 0 , \tag{31}$$

where $\boldsymbol{\lambda} \in \mathbb{C}^n$ is the vector of eigenvalues with a corresponding vector $\boldsymbol{\zeta} \in \mathbb{R}^n$ of dampings. The damping $\zeta_i \in \boldsymbol{\zeta}$ of the i'th eigenvalue $\lambda_i \in \boldsymbol{\lambda}$ can be found as

$$\zeta_i = \frac{\mathrm{Re}(\lambda_i)}{\omega_{ni}} \quad \text{with} \quad \omega_{ni} = |\lambda_i| . \tag{32}$$

The controller design is then defined as finding the set of control parameters that yields the maximum of the smallest eigenvalue damping

$$\arg\max_{(G_d,\tau_d)} \min_i \zeta_i . \tag{33}$$

Given this formulation the process of designing the controller can be completely automated using optimization. As the system was assumed to be linear time-invariant it is necessary to redo the design process should the delay parameter change.

4.3. Delayed Feedback for Helicopter Slung Load System

The delayed feedback control is well suited for oscillation damping in complex systems like the helicopter slung load system as it can account directly for possible delays in the signal loop which in this case originates from the vision system. It is important to realize that this control scheme can not be used for stabilizing the helicopter or to track trajectories, but simply to dampen load swing. Therefore, an inner loop controller for the helicopter is assumed as was illustrated in figure 1.

The feedback variables in the helicopter slung load system are the positions of the slung load relative to the helicopter, x_δ and y_δ and the output of the controller is added to the existing reference to the inner loop helicopter controller. The delayed feedback controller is defined in the context of (25) as

$$\tilde{x}_r = x_r + G_d x_\delta(t-\tau) = x_r + G_d l \sin(\theta_w(t-\tau)) , \tag{34}$$

$$\tilde{y}_r = y_r + G_d y_\delta(t-\tau) = y_r + G_d l \sin(\phi_w(t-\tau)) . \tag{35}$$

Given a full reference trajectory the velocity reference are found as time derivatives of (34) and (35)

$$\dot{\tilde{x}}_r = \dot{x}_r + G_d l \cos(\theta_w(t-\tau_d))\dot{\theta}_w(t-\tau) , \tag{36}$$

$$\dot{\tilde{y}}_r = \dot{y}_r + G_d l \cos(\phi_w(t-\tau_d))\dot{\phi}_w(t-\tau) . \tag{37}$$

Assuming purely slung load dynamics this means that the controller gain G_d can be seen as normalized with respect to the pendulum length. Furthermore, the controller delay is defined as normalized with respect to the pendulum oscillation period T_n

$$\tau_d = T_n \tau_n , \tag{38}$$

where

$$T_n = 2\pi\sqrt{\frac{l}{g}} . \tag{39}$$

Since both controller parameters are defined as normalized to the pendulum length the controller can be designed for one suspension length and when the length is changed, the controller is automatically redesigned accordingly. This should in theory mean that the same oscillation damping is achieved for any suspension length, but in many cases the helicopter dynamics are so slow compare to the pendulum modes that they cannot be neglected. In these cases it is necessary to do a full redesign of the controller for each wire length.

5. Results

The control scheme will here be illustrated use on a small scale autonomous helicopter: The Aalborg University Corona Rapid Prototyping Platform. The AAU Corona is a 1 kg electric indoor helicopter flying with a 0.15 kg slung load in a single 1.25 m wire. It performs fully autonomous flight with landings and takeoff using a set of gain-scheduled PID controllers. A small 320x240 pixel downwards looking camera is mounted on the helicopter for the vision system with a 30^o FOV. There is no computer onboard the helicopter and all control and estimation computation is done on ground in real time. Sensor information from the helicopter is transmitted to the ground though a wired USB connection that hangs from the nose of the helicopter and control signals to the servos are transmitted through the standard radio control system. Furthermore, helicopter and slung load state measurements are acquired using a Vicon motion tracking system at 100 Hz and with a sufficient accuracy for these to be considered as truth measurements. The motion tracking system is only used for verification purposes and not in the slung load control feedback loop.

5.1. Design for Aalborg University Corona

The design for the Corona will only be shown for the lateral dynamics but the process is similar for the longitudinal dynamics. The AAU Corona is controlled by a PID control setup and its dynamic response is close enough to the slung load dynamics that the feedback controller needs redesign for each wire length.

The damping map for a wire length of 1.25 m is shown in figure 12 and the delayed controller parameters is found by the means of a steepest descent method to

$$G_{d,lat} = 0.3\,, \tau_{n,lat} = 0.13\,.$$

The effect of the designed controller on the system dynamics are illustrated in figure 13 Both the estimator and the input shaper do not require any special design as they are independent of the helicopter dynamics.

Figure 11: The Aalborg University Corona flying indoor with slung load.

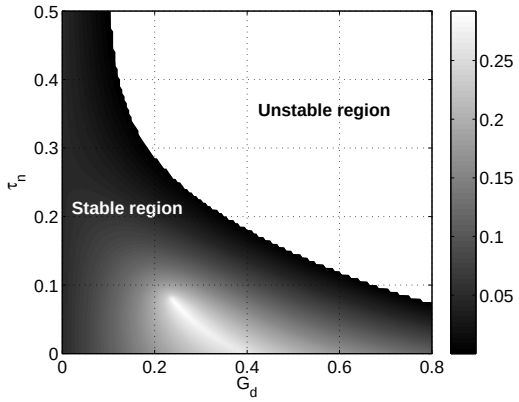

Figure 12: Damping of the lateral helicopter slung load system as a function of delayed feedback controller parameters.

5.1.1. Controller Enable Procedure

The procedure for enabling the controller is

Step 1. The helicopter takes off and lifts the slung load off the ground.

Step 2. The vision system detects the slung load and enables the wire length estimator.

Step 3. The wire length estimator has converged and the result is used in the state estimator and input shaper.

Step 4. The wire length is used to calculate the system dynamics; the values for the delayed controller is found through a steepest descent search

Step 5. The delayed controller is enabled and thereby the full control scheme is running

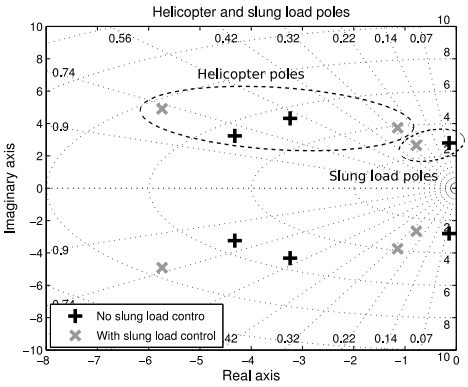

Figure 13: Pole location for the helicopter slung load with and without delayed feedback.

5.2. Estimator Verification

To verify the design of the estimator and test the performance of it, a flight test has been carried out using a number of very aggressive steps.

Two tests are presented; one with gentle motions to see how the filter converges and tracks, and one with an aggressive step where the load swings outside the FOV of the camera to test how well the filter can propagate without measurements.

This test starts with a take-off where the load is lifted off the ground by the helicopter. This means that before the load is dragged under the helicopter, the vision system cannot see the load. This can be observed in the first couple of seconds in figure 14 where the estimate is fluctuating. After that the vision system sees the

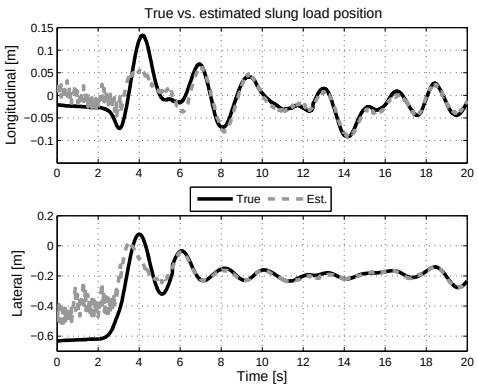

Figure 14: Estimated and true slung load position during takeoff. Note that the true states actually are high quality measurements from the motion tracking system.

slung load and the estimated states starts to converge. However, it takes some seconds before the estimates are tracking satisfactorily – this is due to the fact that the estimator is started with a wrong wire length and first needs to adjust for this. The convergence of the wire length estimator can be seen in figure 15 together with the time between available measurements from the vision system. When the first measurement is available from the vision system the wire length estimator is automatically started with an update frequency of 1 Hz and when it has converged satisfactorily the wire length is locked to the converged value. When looking at both

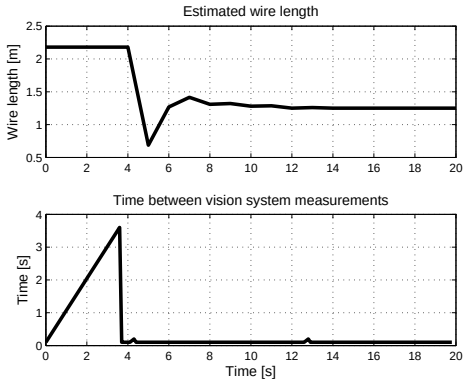

Figure 15: Estimated wire length and time between vision system measurements during takeoff. When the vision system cannot track the slung load, the time between measurements increases.

position and velocity estimates (figure 14 and 16) it can be seen that estimator converge rapidly and tracking the states satisfactorily.

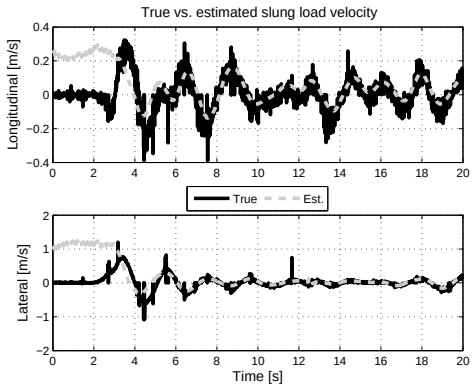

Figure 16: Estimated and true slung load velocities during takeoff

This test is run with an already converged estimator and consists of an aggressive 0.8 m right step with the helicopter. The purpose of this is to create a large enough swing and/or a large enough tilt of the helicopter for the load to disappear out of the picture. The esti-

mated and true position and velocity are shown in figure 17 and 18, from where it can be seen that the estimator is capable of propagating the estimates nicely during the period without measurements (cf. figure 19). The

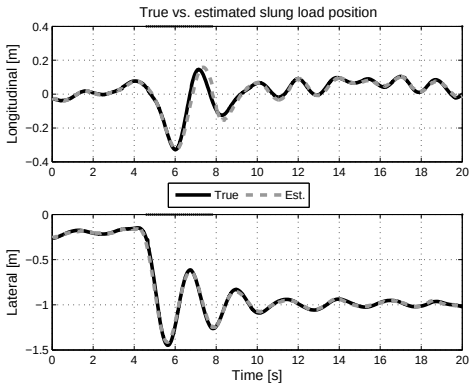

Figure 17: Estimated and true slung load position during aggressive step. The black dots on top of each plot indicates missing vision system measurements.

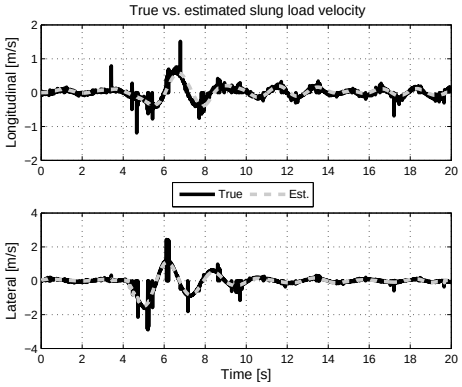

Figure 18: Estimated and true slung load velocities during aggressive step.

measured helicopter accelerations used as input to the process model in this test is shown in figure 20.

5.3. Controller Verification

To illustrate the damping effect of the delayed feedback controller on the AAU Corona two different 1 m lateral manoeuvres are used: A gentle and an aggressive one. The aggressive manoeuvre is simply a step in position reference, while the gentle one is an acceleration and velocity limited s-curve. The steps are performed both with and without the delayed feedback controller and a comparison is shown in figure 21 and 22. As expected the delayed controller is capable of introducing a

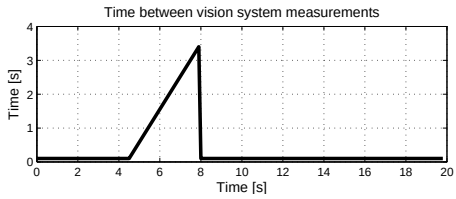

Figure 19: Time between vision system measurements during aggressive step.

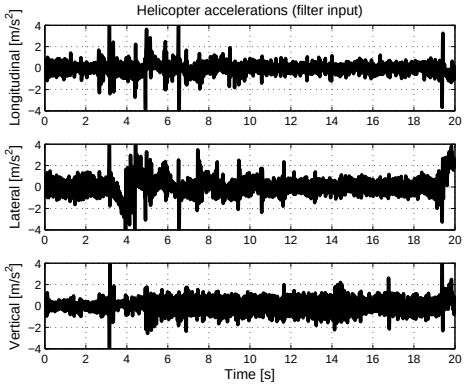

Figure 20: Helicopter acceleration used as filter input during aggressive step.

significant damping improvement with respect to slung load swing.

Finally, to illustrate the combined effectiveness of the delayed feedback and the input shaper, an aggressive step with both controllers enabled is shown in figure 24 and 25. Here, a ZVD input shaper is used to shape the step into a zero residual vibration manoeuvre as is evident on the shaped reference. It can be seen the combination of actively damping swing and avoiding exciting swing during movement results in an almost swing-free motion.

6. Discussion

It is clear that the control scheme is capable of providing considerable damping of the slung load swing compared to flight without a dedicated slung load controller. There is no doubt that the controller is capable of avoiding slung load swing almost completely. However, the cost is an additional maneuver time – for short maneuver as shown in the results, the rest to rest time for the helicopter is almost twice as long with the shaper compared to without. When looking at the results it would be natural to draw the conclusion that the better damping comes simply from the slower helicopter

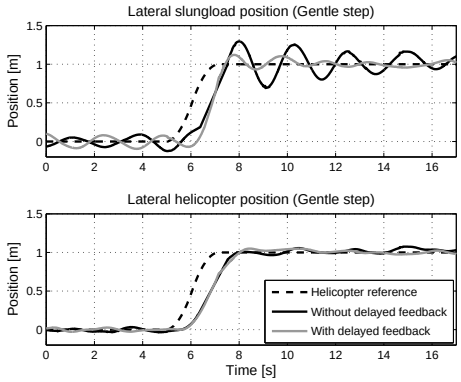

Figure 21: 1 m gentle lateral step with and without delayed feedback.

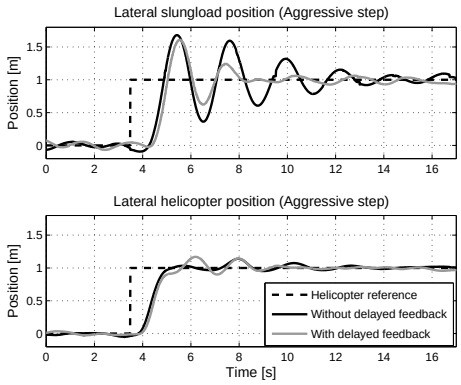

Figure 22: 1 m aggressive lateral step with and without delayed feedback.

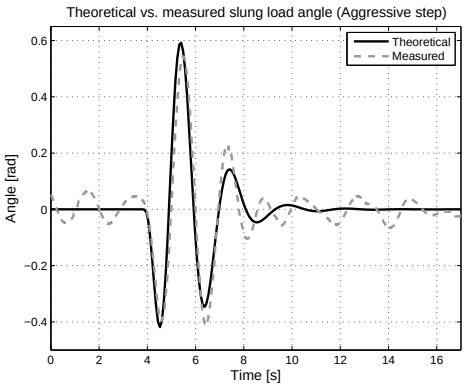

Figure 23: Comparison of theoretical and measured slung load angle during aggressive lateral step with delayed feedback.

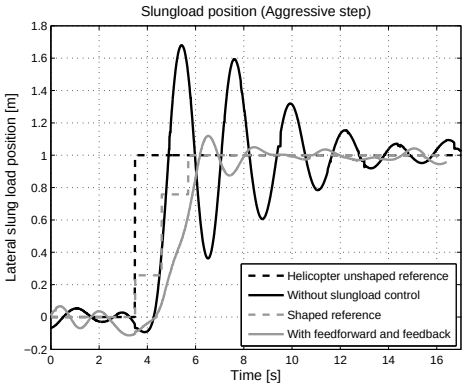

Figure 24: Slung load motion for 1 m aggressive step with and without delayed feedback and input shaping.

response. However, while slower helicopter motion potentially can result in oscillations with smaller amplitude, the input shaper ensures that almost all residual oscillations are removed. Furthermore, the input shaper works for all inputs, slow and fast, and the added maneuver time is the same for all inputs. Both the feedforward and the feedback ultimately alters the trajectory of the helicopter to avoid and dampen load swing and depending on the application these changes could in some cases be unacceptable. A possibility for improvement on the design method could therefore be to integrate a design factor that directly allows a weighting between trajectory changes and slung load swing level.

The input shaping can be robustified against errors in system damping and oscillation frequency through sacrifice of system response time. For the delayed feedback controller the robustness qualities are more modest and while a robustifying modification to the design method is proposed in this paper, further attention to this issue is recommended.

7. Conclusion

In this paper a swing damping control scheme was developed to improve slung load flight in autonomous helicopters. It is designed as an integrated observer and controller scheme and to augment helicopter stand alone controllers. A feedforward control scheme based on input shaping was design to shape trajectories to the system in such a way that ideally excitation of slung load swing through manoeuvring is avoided. A feedback control scheme based on delayed feedback was designed to actively dampen out slung swing and when using both simultaneously, virtually swing free slung load flight can be achieved.

The performance of the control scheme was evaluated through flight testing and it was found that the control scheme is capable of yielding a significant reduction in slung load swing over flight without the controller scheme.

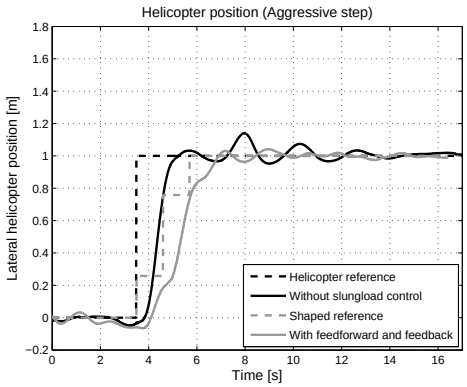

Figure 25: Helicopter motion 1 m aggressive step with and without delayed feedback and input shaping.

References

[1] Baker Jr, G. A., Graves-Morris, P., 1996. Padé Approximants. *Cambridge University Press*.

[2] Ballard, D. H., 1978. Genralizing the Hough Transform to Detect Arbitrary Shapes. *Pattern Recognition, 13, 111-122*.

[3] Banerjee, A., Pedreiro, N., Singhose, W., 2001. Vibration Reduction for Flexible Spacecraft Following Momentum Dumping with/without Slewing. *American Control Conference*.

[4] Bernard, M., Kondak, K., Hommel, G., 2008. A Slung Load Transportation System Based on Small Size Helicopters. *8th International Workshop on Autonomous Systems Self-Organization, Management, and Control*.

[5] Bisgaard, M., 2008. Modeling, Estimation, and Control of Helicopter Slung Load System. *Aalborg University*, PhD Thesis.

[6] Bisgaard, M., Vinther, D., Østergaard, K., Bendtsen, J., Izadi-Zamanabadi, R., 2005. Sensor Fusion and Model Verification for a Mobile Robot. *16th IASTED International Conference on Modelling and Simulation*.

[7] Dukes, T. A., 1973. Maneuvering Heavy Sling Loads Near Hover Part I: Damping the Pendulous Motion. *Journal of the American Helicopter Society, 18, 2-11*.

[8] Dukes, T. A., 1973. Maneuvering Heavy Sling Loads Near Hover Part II: Some Elementary Maneuvers. *Journal of the American Helicopter Society, 18, 2-11*.

[9] Elmali, H., Renzulli, M., Olgac, N., 2000. Experimantal Comparision of Delayed Resonator and PD Controlled Vibration Absorbers Using Electromagnetic Actuators. *Journal of Dynamic Systems, Measurement, and Control, 122, 514-520*.

[10] Faille, D., Weiden, A. J. J. v. d., 1995. Robust regulation of a flying crane. *The 4th IEEE Conference on Control Applications*.

[11] Gupta, N. K., Bryson, Jr., A. E., 1976. Near-Hover Control of a Helicopter with a Hanging Load. *Journal of Aircraft, 13, 217-222*.

[12] Hoh, R. H., Heffley, R. K., Mitchell, D. G., 2006. Development of Handling Qualities Criteria for Rotorcraft with Externally Slung Loads. *NASA*.

[13] Julier, S. J., Uhlmann, J. K., 1997. A New Extension of the Kalman Filter to Nonlinear Systems. *University of Oxford*.

[14] Masoud, Z. N., Daqaq, M. F., Nayfeh, A. H., 2004. Pendulation Reduction on Small Ship-Mounted Telescopic Cranes. *Journal of Vibration and Control, 10, 1176-1179*.

[15] Masoud, Z. N., Nayfeh, A. H., 2003. Sway Reduction on Container Cranes Using Delayed Feedback Controller. *Journal of Nonlinear Dynamics, 34, 347-358*.

[16] Miller, R., Mettler, B., Amidi, O., 1997. Carnegie Mellon University's 1997 International Aerial Robotics Entry. *Association for Unmanned Vehicle Systems International*.

[17] Mittal, M., Prasad, J., Schrage, D., 1991. Nonlinear adaptive control of a twin lift helicopter system. *IEEE Control Systems Magazine, 11, 39-45*.

[18] Oh, S.-R., Ryu, J.-C., Agrawal, S. K., 2006. Dynamics and Control of a Helicopter Carrying a Payload Using a Cable-Suspended Robot. *Journal of Mechanical Design, 128, 1113-1121*.

[19] Olgac, N., Holm-Hansen, B. T., 1994. A Novel Active Vibration Absorption Technique: Delayed Resonator. *Journal of Sound and Vibration, 176, pp. 93-104*.

[20] Raz, R., Rosen, A., Ronen, T., 1989. Active Aerodynamic Stabilization of a Helicopter/Sling-Load System. *Journal of Aircraft, 26, 822-828*.

[21] Reynolds, H., Rodriguez, A., 1992. $\mathcal{H}_\infty$ control of a twin lift helicopter system. *The 31st IEEE Conference on Decision and Control*.

[22] Rodriguez, A. A., Athans, M., 1986. Multivariable control of a twin lift helicopter system using the LQG/LTR design methodology. *Laboratory for Information and Decision Systems, Massachusetts Institute of Technology*.

[23] Schierman, J. D., Ward, D. G., Monaco, J. F., Hull, J. R., 2000. On-line identification and nonlinear control of rotorcraft/external-load systems. *AIAA Guidance, Navigation, and Control Conference and Exhibit*.

[24] Singer, N. C., 1983. Residual Vibration Reduction in Computer Controlled Machines. *Massachusetts Institute of Technology*, phD Thesis.

[25] Singh, T., Singhose, W., 2002. Tutorial on Input Shaping/Time Delay Control of Maneuvering Flexible Structures. *American Control Conference*.

[26] Smith, O. J. M., 1957. Posicast Control of Damped Oscillatory Systems. *Proceedings of the IRE, 45, 1249-1255*.

[27] Udwadia, F. E., Phohomsiri, P., 2005. Active Control of Structures using Time Delay Positive Feedback Proportional Control Designs. *Journal of Structural Control and Health Monitoring, 13, 536-552*.